



ENSO variability and teleconnections during glacial climates

Ute Merkel^{a,*}, Matthias Prange^{a,b}, Michael Schulz^{a,b}

^a MARUM – Center for Marine Environmental Sciences, Leobener Str., D-28334 Bremen, Germany

^b Faculty of Geosciences, University of Bremen, Klagenfurter Str., D-28334 Bremen, Germany

ARTICLE INFO

Article history:

Received 14 December 2008

Received in revised form

1 October 2009

Accepted 6 November 2009

ABSTRACT

Understanding the origin of sub-Milankovitch and millennial-scale abrupt climate change still poses a major challenge. An important role of communicating the orbital-scale forcing into abrupt climate change on millennial and centennial timescales has been hypothesized for the tropics in earlier studies based on the assumption of stationary teleconnections. This paper presents a modelling study for the Last Glacial Maximum and Marine Isotope Stage 3 using the comprehensive climate model CCSM3. Glacial boundary conditions and freshwater hosing at high latitudes of the North Atlantic are imposed to mimic a Heinrich stadial and Dansgaard-Oeschger stadials and interstadials. It is shown that glacial ENSO variability is strongly enhanced by a substantial slowdown of the Atlantic Meridional Overturning Circulation. The simulations also suggest that glacial boundary conditions induce major modifications to ENSO teleconnections and that the “blueprint” of modern ENSO teleconnections should only be applied with caution to glacial climate periods.

© 2009 Elsevier Ltd. All rights reserved.

1. Introduction

The oscillatory nature of the tropical Pacific El Niño–Southern Oscillation (ENSO) phenomenon and the widespread global climate anomalies concomitant with interannual ENSO extremes (El Niño, La Niña events) provide a challenge for a more thorough understanding of ENSO dynamics and the ability to better forecast ENSO extremes. In these respects, much progress has been made during recent decades (Latif et al., 1998; Dommenges and Stammer, 2004; Guilyardi et al., 2009). The picture is less clear, however, for different background climatic states. Both for anthropogenically induced future climate change (Timmermann et al., 1999; Collins et al., 2005; van Oldenborgh et al., 2005; Guilyardi, 2006; Merryfield, 2006; Guilyardi et al., 2009) and for past climates (Koutavas et al., 2002) such as the last glacial, a different behavior of the tropical Pacific ocean–atmosphere coupled system has been hypothesized. However, the exact nature of the ENSO response to modified boundary conditions has not yet been fully understood. Indeed, proxy-based reconstructions and results from coupled ocean–atmosphere models show a large variety of results.

Although clear proxy evidence for past ENSO behavior is often hampered by the lack of adequate temporal resolution of the proxy records, several indications have been reported emphasizing

a clearly non-stationary picture of tropical Pacific climate. Coral records and reconstructions from foraminifera shells suggest external controls of tropical Pacific climate ranging from orbital to millennial and submillennial timescales (Tudhope et al., 2001; Stott et al., 2002; Rein et al., 2005; Pena et al., 2008).

Fully comprehensive general circulation models of the coupled ocean–atmosphere–sea–ice system have been used to study past ENSO behavior. For instance, simulations with an earlier version (CSM1.4) of the Community Climate System model (CCSM) revealed an increase of ENSO variability at the Last Glacial Maximum (LGM; Otto-Bliesner et al., 2003; Peltier and Solheim, 2004). Subsequently, Otto-Bliesner et al. (2006a) conducted an LGM simulation with version 3 of the CCSM. This experiment showed weaker ENSO variability which demonstrates that ENSO behavior in a different background climate may be model-dependent. ENSO behavior at the LGM thus remains rather inconclusive as is further confirmed by an intercomparison of several LGM simulations (Zheng et al., 2008).

During recent years, it has been frequently discussed whether the ENSO phenomenon is possibly connected to changes in the Atlantic Ocean meridional overturning circulation (AMOC). Zhang and Delworth (2005), for instance, have shown in their freshwater-hosing study using the GFDL coupled general circulation model (GCM) that a pronounced slackening of the AMOC impacts on the eastern tropical Pacific mean state and thus probably on the annual cycle which is supposed to interact with interannual ENSO variability (Jin et al., 1994; Tziperman et al., 1994). The response of ENSO variability itself to a reduction of the Atlantic Ocean

* Corresponding author. Tel.: +49 421 218 65440; fax: +49 421 218 65454.

E-mail addresses: umerkel@marum.de (U. Merkel), mprange@marum.de (M. Prange), mshulz@marum.de (M. Schulz).

overturning has been described in the framework of an intermediate complexity model (Timmermann et al., 2005) and in a coupled GCM intercomparison (Timmermann et al., 2007b) indicating a strengthening of ENSO in 4 out of 5 state-of-the-art models. In these cases, an important link is provided by intensified northeasterly trade winds communicating the signal from the Atlantic to the eastern equatorial Pacific Ocean.

Beyond changes in tropical Pacific variability, also ENSO teleconnections can be subject to modifications due to a different background climate. In future climate scenario runs with the ECHAM5/MPI-OM model, strong connections between changes of the mean state and changes in the teleconnection patterns associated with El Niño events are found (Müller and Roeckner, 2008). Similarly, ENSO teleconnections can be expected to respond to glacial climate boundary conditions. It has been suggested that during the last glacial period, continental ice sheets exerted a major control on atmospheric dynamics. Specifically, ice sheets alter the position of the atmospheric jetstreams and the mid-latitude stormtracks (e.g. Laine et al., 2008) which, in turn, can be expected to induce a complex interplay with the tropical-extratropical atmospheric bridge.

ENSO variability and ENSO teleconnections have also been suggested to respond to Milankovitch forcing (Clement and Cane, 1999; Clement et al., 1999). In these studies, it has been hypothesized that changes in the Atlantic Ocean overturning circulation by itself are insufficient to induce abrupt climate change beyond the Atlantic realm. Accordingly, the tropics may play a decisive role in communicating orbital signals globally and triggering abrupt climate changes at millennial timescales and glacial-interglacial cycles (Clement and Cane, 1999; Cane and Clement, 1999; Clement and Peterson, 2008). This hypothesis is based on the assumption of stationary teleconnections from the tropics to the extratropics and does not consider glacial boundary conditions such as continental ice sheets.

With respect to this hypothesis, the following questions still remain to be answered:

1. Is ENSO variability responding to glacial boundary conditions and glacial changes in the Atlantic Ocean overturning circulation?
2. Can the modern ENSO teleconnection patterns be used as a “blueprint” for interpreting abrupt climate change during the Late Quaternary?

This study addresses these questions using a comprehensive coupled climate model, focussing on the LGM and Marine Isotope Stage 3 (MIS3, 59 ka BP–29 ka BP). MIS3 in particular is a very prominent period in climate history with pronounced millennial-scale climate shifts such as Heinrich and Dansgaard-Oeschger (DO) events (see Sarnthein et al., 2001, for a review) involving pronounced sea-level changes (Siddall et al., 2003; Arz et al., 2007; Rohling et al., 2008; Siddall et al., 2008). So far, the climate of MIS3 has only been investigated with uncoupled atmospheric GCMs (Barron and Pollard, 2002) or coupled intermediate complexity models such as CLIMBER (Jin et al., 2007) and LOVECLIM (van Meerbeek et al., 2009). Our simulations are designed to mimic the LGM, Heinrich Stadial 1 (HS1) and a generic Dansgaard-Oeschger stadial and interstadial by prescribing glacial boundary conditions and perturbations of the ocean freshwater budget in the North Atlantic. Detailed results of our MIS3 simulations will be described elsewhere. In this study, we focus on how different glacial climatic states affect ENSO variability and the associated ENSO teleconnections.

The paper is organized as follows. In the next section, we will give an overview of our experimental framework of glacial climate

simulations. Major characteristics and results from these simulations will be described in Section 3. Subsequently, the response of ENSO variability and changes in ENSO teleconnections in different glacial background states are reported. Implications of these findings will be discussed in the final chapter.

2. Model and experiments

In our study, the comprehensive Community Climate System Model Version 3 (CCSM3; Collins et al., 2006) has been used. It consists of state-of-the-art representations of the atmosphere, ocean, land and sea-ice components. The model has participated successfully in international initiatives such as the Paleomodelling Intercomparison Project (Braconnot et al., 2007a) and delivered future climate scenario runs to the Intergovernmental Panel on Climate Change (IPCC) assessment reports. To allow longer integration times, our model experiments have been performed with the low-resolution CCSM3 model setup as described by Yeager et al. (2006). The model runs have been conducted at a spectral truncation of T31 (3.75° by 3.75°) with a vertical discretization of 26 levels for the atmosphere model. The ocean and sea-ice components are nominally run on a 3° grid with 25 levels in the ocean. The ocean model has an equatorial refinement to a horizontal resolution of about 0.9°. The low-resolution setup of the model exhibits no significant degradations with respect to T42 resolution (Yeager et al., 2006). With respect to the CCSM3 model's performance in representing ENSO in general, the reader is referred to Deser et al. (2006). For modern boundary conditions, the performance of the low-resolution version has been studied by Yeager et al. (2006) and Otto-Bliesner et al. (2006b). These studies conclude that the most important shortcomings of CCSM3 with respect to ENSO are found in the eastern upwelling regions and in the simulation of the annual cycle. ENSO variability is too high-frequency, too low in the eastern tropical Pacific and its maximum is shifted towards the central equatorial Pacific. These imperfections, however, are not a resolution problem and can be found in many state-of-the-art comprehensive climate models (see Guilyardi et al., 2009, for a review).

Our experimental framework is summarized in Table 1 and comprises four glacial climate simulations:

- (i) A baseline simulation for the LGM (21 000 years before present) following the guidelines of the Paleomodelling Intercomparison Project 2 (Braconnot et al., 2007a,b). This LGM simulation takes into account the orbital parameters and the greenhouse gas concentrations of CO₂, CH₄ and N₂O. An LGM sea-level lowering by 120 m has been taken into account by a modification of the land-sea distribution which, for instance, leads to a closure of Bering Strait. In addition, LGM continental ice sheet topography and the corresponding background albedo have been adapted based on the ICE-5G dataset (Peltier, 2004). The simulation covers more than 600 model years in total and has been branched off an existing LGM simulation (Eisenman, 2008).
- (ii) The next experiment we conducted is identical to the LGM simulation of (i) except for a permanent freshwater anomaly of about 0.2 Sv which is distributed over the whole Greenland-Iceland-Norwegian Seas (north of about 65° N) and which is not compensated for elsewhere. Our glacial freshwater hosing experiment contrasts the present-day setup of many other hosing studies (e.g. Stouffer et al., 2006) which do not take into account the glacial boundary conditions. The experiment is initialized from our LGM simulation described above and will be referred to as Heinrich Stadial 1 analogue (HS1 hereafter).
- (iii) A baseline simulation for MIS3 centered on 35 000 years BP has been conducted thereby taking into account the

Table 1
Summary of CCSM3 experiments with the respective boundary conditions and selected key diagnostics.

Experiment	Preindustr. Control	Last Glacial Maximum	Heinrich Stadial 1	MIS3 Stadial	MIS3 Interstadial
Acronym	PI	LGM	HS1	ST	IST
Exp. length [years]	700	640	360	260	290
Continental ice sheets	CCSM3 standard config.	21 ka BP (ICE-5G)	21 ka BP (ICE-5G)	35 ka BP (ICE-5G)	35 ka BP (ICE-5G)
Orbital configuration	1950	21 ka BP	21 ka BP	35 ka BP	35 ka BP
Eccentricity	0.01672393	0.01899384	0.01899384	0.01464555	0.01464555
Obliquity	23.446°	22.949°	22.949°	22.754°	22.754°
Longit. of perihel.	102.04°	114.42°	114.42°	249.58°	249.58°
Greenhouse gas conc.					
CO ₂ [ppmv]	280	185	185	205	205
N ₂ O [ppbv]	270	200	200	225	225
CH ₄ [ppbv]	760	350	350	550	550
Glob. avg. temp. [K]	285.9	281.8	281.4	281.8	282.5
AMOC (25°S) [Sv]	11.6	10.1	2.7	6.6	14.1
Reference experiment	PI	LGM	LGM	LGM	ST

corresponding 35 ka BP orbital parameters and greenhouse gas concentrations of CO₂, CH₄ and N₂O (Flückiger et al., 2004; Spahni et al. 2005; Ahn and Brook, 2007) (see Table 1). The focus on 35 ka BP is motivated by the fact that this timeslice lies within a period of rather regular Dansgaard-Oeschger variability. Furthermore, the 35 ka BP continental ice sheet topography based on the ICE-5G dataset (Peltier, 2004) has been implemented into the simulation which is branched off the baseline LGM simulation. This experiment is referred to as Dansgaard-Oeschger stadial (ST) analogue.

- (iv) In order to mimic a Dansgaard-Oeschger interstadial (IST), an interstadial simulation for MIS3 also centered on 35 000 years BP has been performed. The setup of this simulation is identical to (iii) except for a permanent negative freshwater forcing of -0.1 Sv over the Greenland-Iceland-Norwegian Seas. The integration has been branched off the 35 ka BP stadial simulation. As described in the next section, the extraction of freshwater from the North Atlantic is an ad-hoc approach to reinvigorate the AMOC from its weak stadial state simulated in the ST experiment. This was motivated by paleoceanographic reconstructions that point to the close link between changes in AMOC strength and stadial-to-interstadial transitions (e.g. Sarin et al., 2001). Due to the coarse resolution of the model, the difference in sea-level of about 60 m between LGM and 35 ka BP has not been taken into account here.
- (v) We also conducted a control simulation with preindustrial (PI) boundary conditions. The setup corresponds to the standard CCSM3 model (Yeager et al., 2006). As to the preindustrial boundary conditions, the total solar irradiance, greenhouse gas concentrations, and aerosol distributions are taken into account according to the guidelines for PI simulations within PMIP2 (Braconnot et al., 2007a). We note that the solar irradiance, the ozone and aerosol distributions in our glacial experiments are the same as in the PI simulation.

The last 100 years of each simulation are retained for analysis and discussed in the remainder of this paper. Each simulation has been run long enough to bring 100-year trends, for instance of the strength of the AMOC, to values close to equilibration. Pacific temperature trends are about 0.1 °C/100 years or less in the upper 500 m in the various simulations except for IST (0.15 °C/100 years) which we consider sufficiently small for the focus of this study.

It is important to note that our LGM simulations (with and without freshwater forcing) differ from the CCSM3 LGM simulations described in Otto-Bliessner et al. (2006a) and Hu et al. (2008) with respect to the model resolution. In addition, the amplitude of our glacial freshwater forcing is at the lower side of the range of

values used in Stouffer et al. (2006). Furthermore, the freshwater forcing is different from that in the study by Bitz et al. (2007) who applied an instantaneous salinity forcing to the upper ocean column. It also differs from the recent study by Hu et al. (2008), who prescribed a much stronger freshwater anomaly of 1 Sv to the model. However, our freshwater forcing lies in the range of freshwater input needed to explain the sea-level changes reconstructed for Heinrich stadials (Chappell, 2002; Siddall et al., 2003).

3. Mean climate changes

The CCSM3 LGM simulation is characterized by a global mean surface cooling of about 4 K with respect to preindustrial conditions (Table 1). This is in very good agreement with the results of the CCSM3 LGM simulation at T42 resolution by Otto-Bliessner et al. (2006a). The cooling is particularly prominent at high latitudes and predominant over the continents. But also over the oceans, in particular in the North Atlantic area and in the Southern Ocean south of 30°S, glacial surface temperatures are significantly reduced (Fig. 1a). Forcing the North Atlantic Ocean with the 0.2 Sv freshwater input (HS1) generates the well-established interhemispheric see-saw characteristic (Fig. 1b) which has been described in many waterhosing experiments under present climate conditions (e.g. Stouffer et al., 2006). The opposite polarity between hemispheres in the HS1 temperature response can account for global average temperatures differing only marginally between LGM and HS1 (Table 1). The MIS3 stadial simulation (ST) does not show a significant global mean temperature change with respect to LGM conditions (Table 1). The LGM and ST simulations differ with respect to the orbital parameters and greenhouse gas concentrations, and the height of the 35 ka BP ice sheets is only half of the LGM height. Therefore, on a global annual mean basis, the effects of the respective 35 ka boundary conditions seem to compensate each other. However, since we do not have simulations with the different 35 ka BP boundary conditions prescribed individually, we are not able to isolate the individual influence of the 35 ka BP ice sheets or 35 ka BP insolation changes separately. The ST simulation exhibits a northern-hemisphere wave-like temperature response compared to LGM conditions (Fig. 1c) which we hypothesize to be mainly due to the different height of the LGM and MIS3 Laurentide and Fennoscandian ice sheets. The ST and IST simulations show slightly different global mean temperatures (Table 1). The IST warming in high northern latitudes is partially compensated by the large areas of weak cooling in the Southern Hemisphere.

In order to better illustrate the mean changes in the tropical Pacific in the respective simulations, Fig. 1 is reproduced with a focus on the tropical Pacific region (Fig. 2). For the discussion in

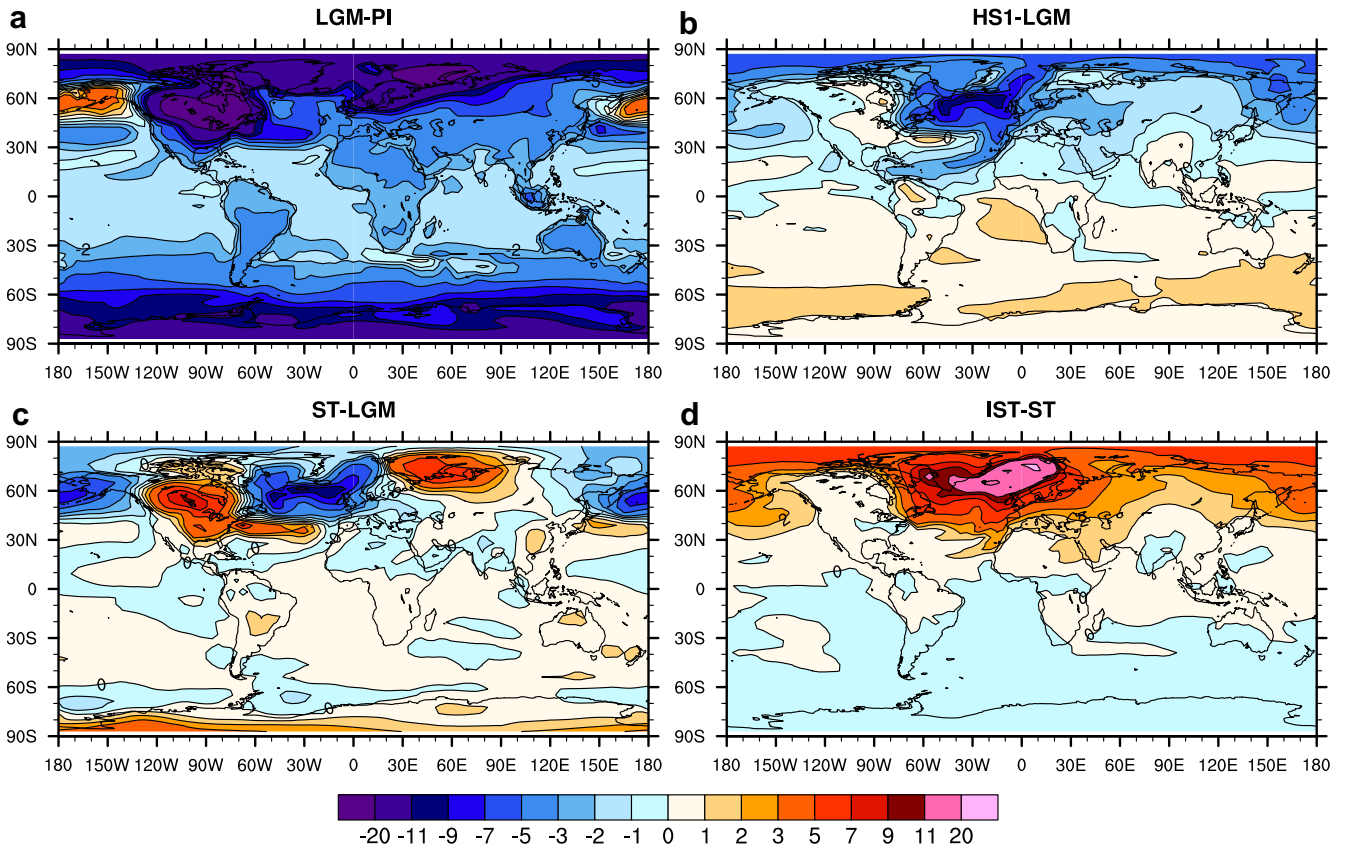


Fig. 1. Annual mean response of surface temperature (K): a) LGM with respect to preindustrial control, b) Heinrich Stadial 1 with respect to LGM, c) stadial with respect to LGM, d) interstadial with respect to stadial simulation. Results are based on the last 100 years of each simulation. Note the irregular contour intervals.

the next section, it is important to note that multi-year annual mean surface temperature changes in the tropical Pacific amount to a cooling of 1–2 °C at the LGM which is less than the strong cooling found in the LGM simulation by Peltier and Solheim (2004). The

eastern tropical Pacific exhibits a meridional structure with a stronger (weaker) LGM cooling south (north) of the equator. The HS1 simulation shows a pronounced dipole-like response across the equator compared to the LGM experiment, i.e. in response to

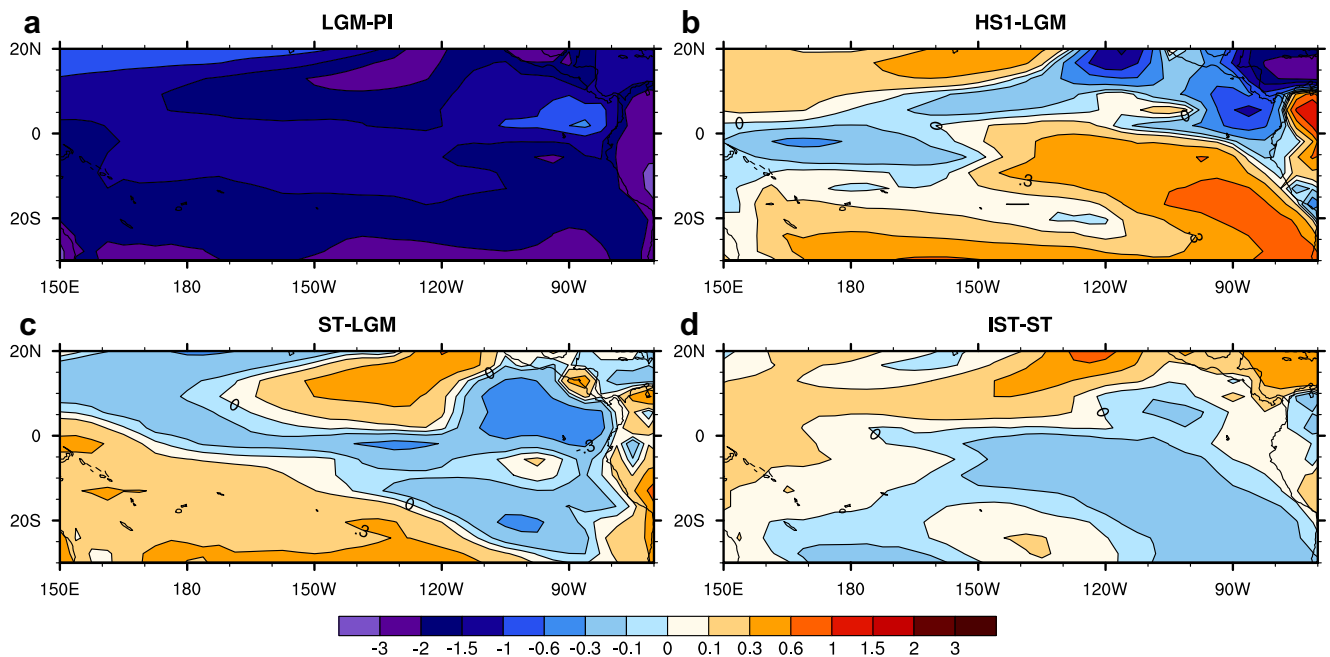


Fig. 2. As Fig. 1, with a focus on the tropical Pacific.

the freshwater hosing (Fig. 2b). This is consistent with the response found in modern hosing simulations discussed by Timmermann et al. (2007b, their Fig. 4). Changes in the tropical Pacific are also well pronounced in our ST (Fig. 2c) simulation. Here, the north-eastern tropical Pacific cooling with respect to LGM conditions amounts to about 0.5°C . The two MIS3 simulations, ST and IST (Fig. 2d), which only differ in the freshwater extraction from the North Atlantic, show a cooling (warming) south (north) of the equator (Fig. 2d). A comparison of Fig. 2b,d reveals similar shapes and opposite signs of the cross-equatorial temperature changes in response to freshwater hosing and extraction.

The maximum overturning in the North Atlantic is reduced by nearly one third from about 15 Sv in the PI control simulation to about 11 Sv for the LGM (Fig. 3a,b). Furthermore, a shallowing of the overturning cell is simulated by our LGM experiment. This is qualitatively consistent with proxy evidence (Sarnthein et al., 2001; McManus et al., 2004; Lynch-Stieglitz et al., 2007). In response to the disturbance to the freshwater budget of 0.2 Sv, the AMOC weakens considerably within a few decades and equilibrates at about 3.5 Sv (Fig. 3c). With 35 ka BP boundary conditions prescribed, the AMOC strength amounts to about 8 Sv and is interpreted as a stadial climate (ST, Fig. 3d). When freshwater is removed from the North Atlantic by a rate of 0.1 Sv, as imposed in our IST simulation to mimic a Dansgaard-Oeschger-type

interstadial, the AMOC recovers to about the same strength as in the PI experiment (Fig. 3e). However, the Atlantic Ocean overturning cell is much shallower compared to preindustrial climate in favor of the Antarctic bottom water.

The ocean response in the different experiments is summarized in terms of deep-water export from the Atlantic to the Southern Ocean (see Table 1) and identified as the maximum of the AMOC at 25°S and below 500 m depth to exclude the effect of the near-surface Ekman cells. Our ST simulation indicates a clear impact of 35 ka BP versus LGM boundary conditions on the Atlantic overturning which is in contrast to simulations with the LOVECLIM model (van Meerbeek et al., 2009) which shows no pronounced sensitivity of the AMOC. The detailed analysis of changes in the oceanic meridional heat transport and sea ice extent in our simulations will be discussed elsewhere but preliminary analysis shows clear implications of a larger glacial sea-ice extent onto the strength and positions of North Atlantic deep-water formation.

4. Tropical Pacific changes in mean state, annual cycle and variability

Eastern tropical Pacific variability is commonly identified from sea surface temperature (SST) anomalies area-averaged over the Niño3 region (150°W – 90°W , 5°S – 5°N ; Trenberth, 1997) thereby

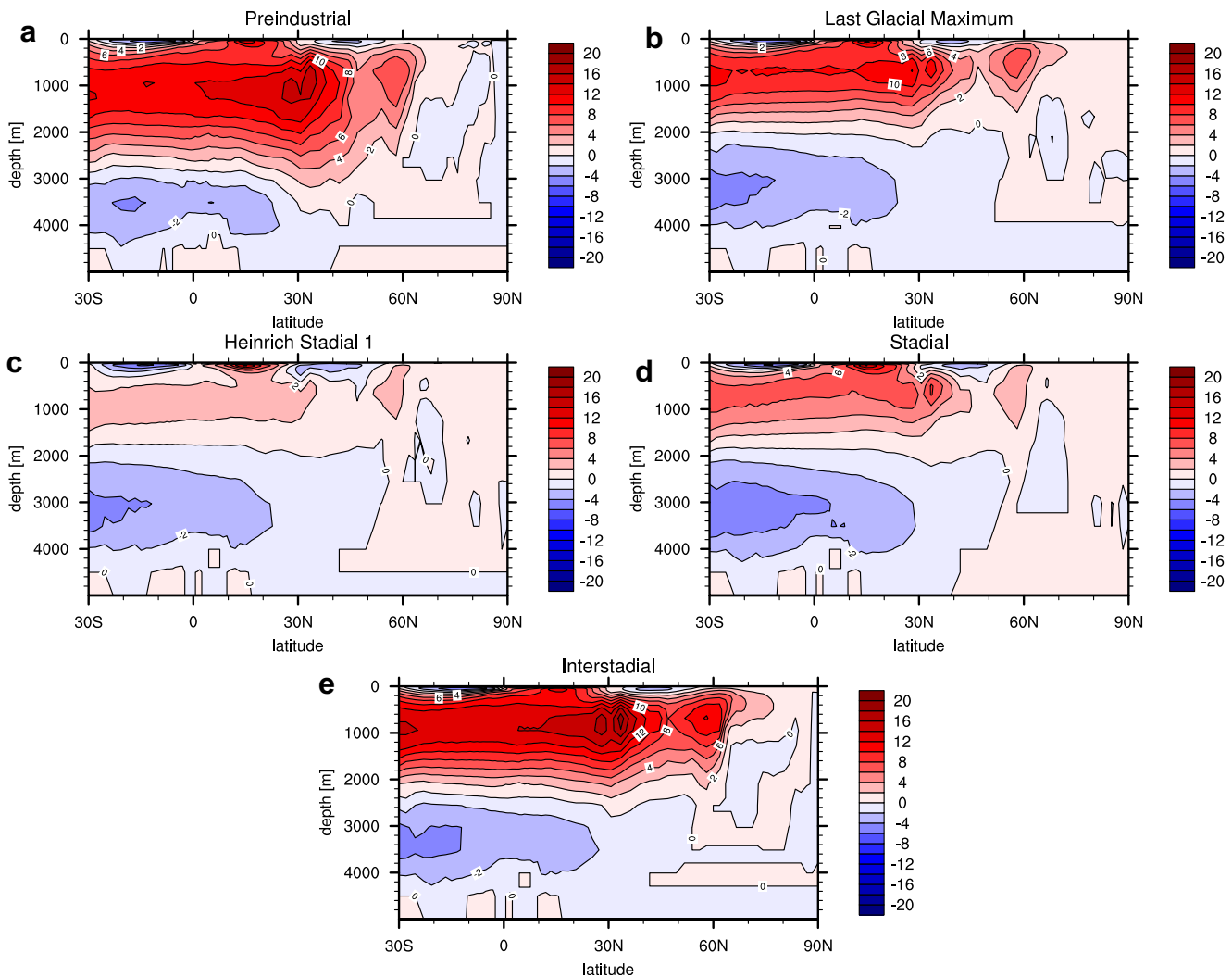


Fig. 3. Atlantic Ocean meridional overturning circulation (Sv, $1 \text{ Sv} = 10^6 \text{ m}^3/\text{s}$) for a) preindustrial control, b) LGM, c) Heinrich Stadial 1, d) stadial, e) interstadial experiments. Note the irregular contour intervals.

removing the mean annual cycle. For each model simulation described above, we calculated the respective monthly Niño3 temperature anomalies. The response of tropical Pacific variability to the different imposed forcings is analyzed from probability density functions determined for each experiment (Fig. 4). This is motivated by the findings of Clement et al. (1999) who described a strong dependency of the number of ENSO events in response to the orbital forcing in their model. Modern frequency distributions of temperature anomalies are known to be skewed towards El Niño events, which exhibit stronger amplitudes than La Niña events (e.g. Trenberth, 1997; Burgers and Stephenson, 1999). Current state-of-the-art models have difficulties in reproducing this observed skewness and show a more symmetric distribution of El Niño and La Niña events (Guilyardi et al., 2009). This is also the case for the CCSM3 model (not shown). However, it is reasonable to assume that this model bias is not dependent on the background climatic state.

With preindustrial forcing, the model seems to be skewed towards more strong La Niña events (Fig. 4a). A more symmetric probability density function arises for LGM conditions (Fig. 4b) with no preference for either strong El Niño events or strong La Niña events. LGM conditions seem to produce a slightly larger number of moderate La Niña events which might be reflected in the mean state cooling described in the previous section. The most prominent change in our whole experimental framework is found in the HS1 simulation (Fig. 4c). Here, a considerable increase in strong ENSO events of either polarity is simulated. The probability density functions for the ST and IST simulations are not significantly different from the control simulation and therefore not presented.

In order to retain the typical interannual ENSO periods, the time series of Niño3 surface temperature anomalies were bandpass-filtered within a range of 1.5–8 years using a 6th-order Butterworth filter and taking into account that the CCSM3 produces a too regular ENSO signal with a typical period of 2 years (Deser et al., 2006). The standard deviation of the bandpass-filtered Niño3 index is used to summarize ENSO variability for all experiments (Fig. 5a). The most significant change in ENSO variability is evident in the HS1 simulation. For present-day waterhosing simulations, Timmermann et al. (2007b) have identified both the mean state and the phase locking with the annual cycle to play an important role in translating the Atlantic signal into tropical Pacific variability changes. Our results suggest that at least part of the mechanisms proposed by Timmermann et al. (2007b) also hold for glacial background

conditions. ENSO variability is rather similar between the LGM, ST and IST simulations (Fig. 5a).

More insight into the glacial changes of ENSO variability is gained by taking into account that ENSO variability is determined by a number of different factors. The sum and interplay of different feedbacks, such as the zonal advective and the thermocline feedback, are responsible for El Niño and La Niña events to grow and for the mechanism of phase transition of the SST anomalies (Jin and An, 1999; Guilyardi et al., 2009). A full exploration of these feedbacks would be beyond the scope of this paper. In particular, it has not yet been fully understood whether state-of-the-art GCMs are actually able to reproduce the same kind of feedbacks as established in linear framework studies (Jin and An, 1999; Fedorov and Philander, 2001). Guilyardi et al. (2009) note that many models tend to underestimate the thermocline feedback which is the effect of thermocline depth variations on SST variability.

Here, we instead focus on a few simple diagnostics that have been identified to be closely related with ENSO variability: the background mean state and the annual cycle.

The meridional asymmetry of surface climatology across the equator is a key factor in determining tropical east Pacific mean climate, annual cycle and variability. In close connection to the seasonal migration of the ITCZ, the cross-equatorial SST gradient in the eastern tropical Pacific drives cross-equatorial winds and essentially sets up the annual cycle in the eastern tropical Pacific (Xie, 1994). The meridional asymmetry may also be affected by changes in the AMOC as shown by present-day freshwater hosing simulations (Timmermann et al., 2007b). In order to quantify how meridional asymmetry responds to the glacial and freshwater forcing in our different simulations, we calculated regional averages of SST for a northern (5°N – 12°N , 150°W – 80°W) and a southern (12°S – 5°S , 150°W – 80°W) Pacific region. The difference between these regional averages is shown in Fig. 5b. In all our simulations, the gradient is positive, i.e. the sea surface north of the equator is warmer than the south. At the LGM, meridional asymmetry is increased compared to PI due to a stronger cooling in the southeastern tropical Pacific (see Figs. 2a and 5b). The most evident change, however, is seen for HS1 where the meridional temperature gradient is reduced by more than 0.6°C compared to the LGM which points to a weakening of the annual cycle compared to the LGM in response to the freshwater hosing. An analogue increase, although weaker in magnitude, in meridional asymmetry is found in the IST simulation (compared to ST) in response to the freshwater extraction.

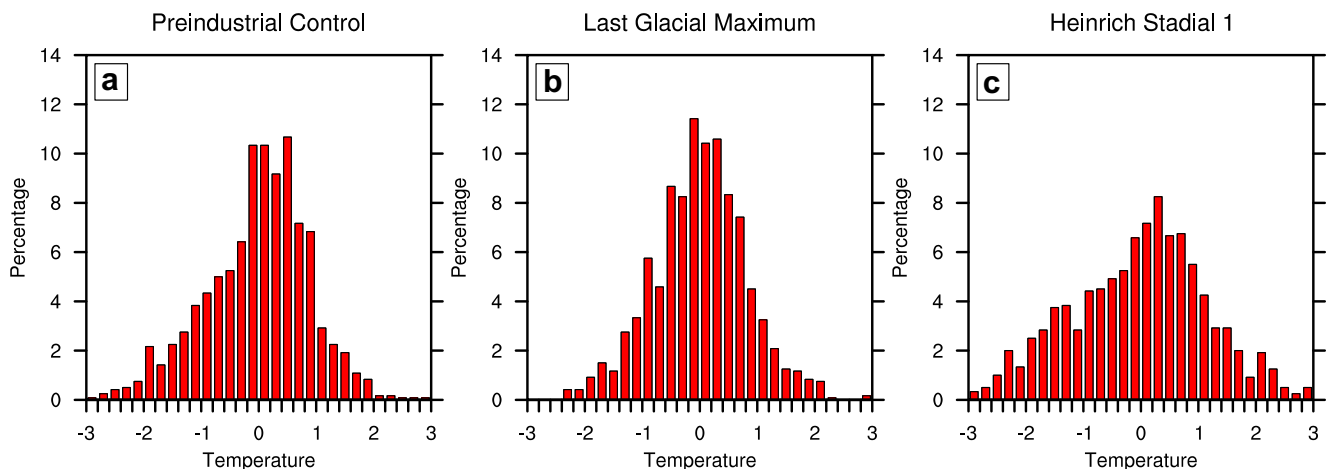


Fig. 4. Probability density functions of the monthly Niño3 surface temperature anomalies after removal of the mean annual cycle for a) the preindustrial control simulation, b) LGM and c) Heinrich Stadial 1.

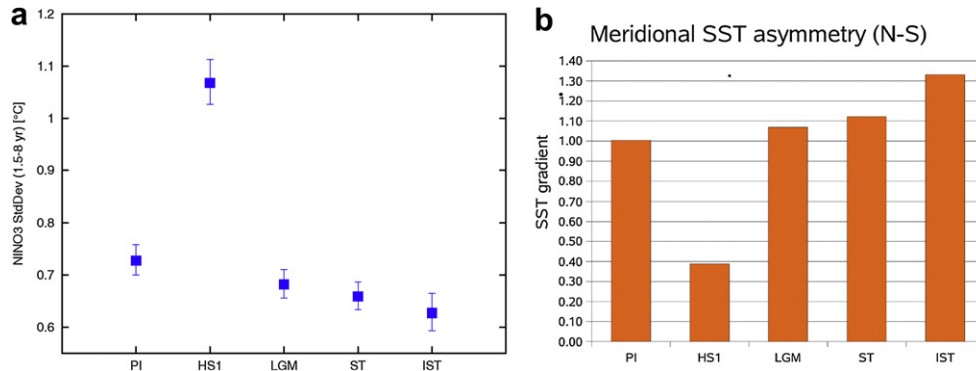


Fig. 5. a) ENSO variability for the different climate states. Shown is the standard deviation of surface temperature anomalies in the Niño3 region, using bandpass-filtered data (1.5–8 yr; 6th-order Butterworth filter). Error bars indicate 95% confidence intervals based on a χ^2 -distribution. b) Meridional asymmetry calculated as the difference between annual mean surface temperature averaged over the northern (5°N–12°N, 150°W–80°W) and southern (12°S–5°S, 150°W–80°W) tropical Pacific, units: K.

As seen from Fig. 5, we find a very good anti-correlation between the strength of ENSO and the meridional asymmetry in all our simulations. Taking into account the relationships of “pronounced meridional asymmetry – strong annual cycle” (Xie (1994)) and “strong annual cycle – weak interannual variability” (Guilyardi, 2006), our results suggest that the variability changes shown in Fig. 5a can partly be explained by changes in the strength of the annual cycle which is consistent with the frequency entrainment mechanism described by Liu (2002) and Timmermann et al. (2007a). This can be further illustrated by means of the annual cycles of Niño3 SST (with the annual mean subtracted) and Niño3 SST standard deviations. As an example, this is shown in Fig. 6 for the LGM and HS1 experiments where the strongest change in variability is simulated. For most months, variability is increased at HS1 compared to LGM (Fig. 6b), while the amplitude of the annual cycle is clearly weaker in the HS1 simulation (Fig. 6a). It should be noted that the peak of the spectra of Niño3 SST for the respective simulation (not shown) remains at a period of about 2 years, and the spectra do not show a shift towards lower or higher frequency. So the 2-year period seems to be a robust characteristic of CCSM3-T31 throughout different climatic states.

So far, only near-surface changes have been discussed. However, ENSO is also strongly determined by subsurface processes through vertical displacements of the thermocline. Mean thermocline depth along the equator is strongly dependent on the strength of the equatorial easterly winds. Therefore, changes in the wind field in different glacial climates should have an impact on the equatorial Pacific thermocline structure. Additionally, based on earlier studies (Huang et al., 2000; Cessi et al. 2004; Timmermann et al. 2005), a readjustment of the global ocean circulation through oceanic waves (“seiching”) must be expected in response to changes in North Atlantic deep-water formation. Since in all our experiments, the meridional overturning circulation is significantly modified, changes in the thermocline structure must be expected accordingly. Therefore we analyzed both the absolute values and the response of the tropical Pacific thermocline depth in the different simulations and compare these to changes in zonal wind stress along the equator (Figs. 7–10). Many studies use the depth of the 20 °C isotherm as an approximation to Pacific thermocline depth. However, in our glacial experimental framework, we found the 17 °C isotherm to better approximate the depth at which the largest vertical density gradients occur.

In the LGM simulation, thermocline has risen (Fig. 7a) in particular over the western and central tropical Pacific resulting in a flattening of the thermocline. This is consistent with the overall weakening of zonal wind stress (Figs. 9a and 10a) and a pronounced weakening of the east-west SST gradient along the equator (not shown).

In response to the HS1 freshwater forcing, a deeper thermocline than at LGM is established over the western and central tropical Pacific, with a slight shoaling over the eastern tropical Pacific (Figs. 7b and 8b). The deepening in the western and central tropical Pacific is consistent with the finding by Cessi et al. (2004) and Timmermann et al. (2005) of an ocean thermocline adjustment to a slowdown of the AMOC. Depth changes are in the range of the results by Timmermann et al. (2007b). The shoaling of the thermocline in the eastern part is consistent with enhanced upwelling and stronger easterlies, and this results in an overall steepening of the thermocline. With 35 ka boundary conditions (ST), the thermocline gets deeper west of 110°W (Figs. 7c and 8c) consistent with the stronger easterly wind forcing (Fig. 9c). Wind stress and

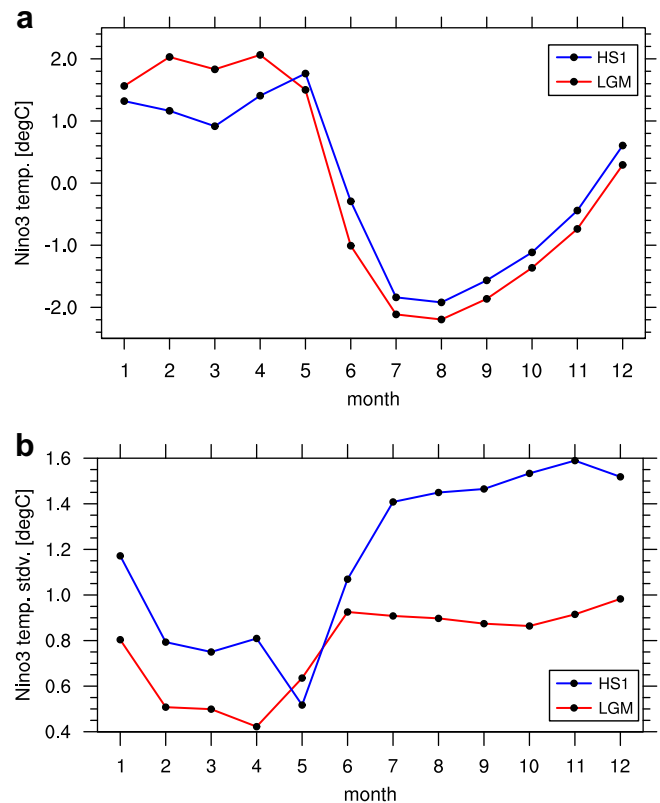


Fig. 6. a) Annual cycle of Niño3 surface temperature anomalies (annual mean removed, units: K). b) Standard deviation of Niño3 surface temperature anomalies as a function of calendar month (units: K). Red (blue) line denotes LGM (HS1).

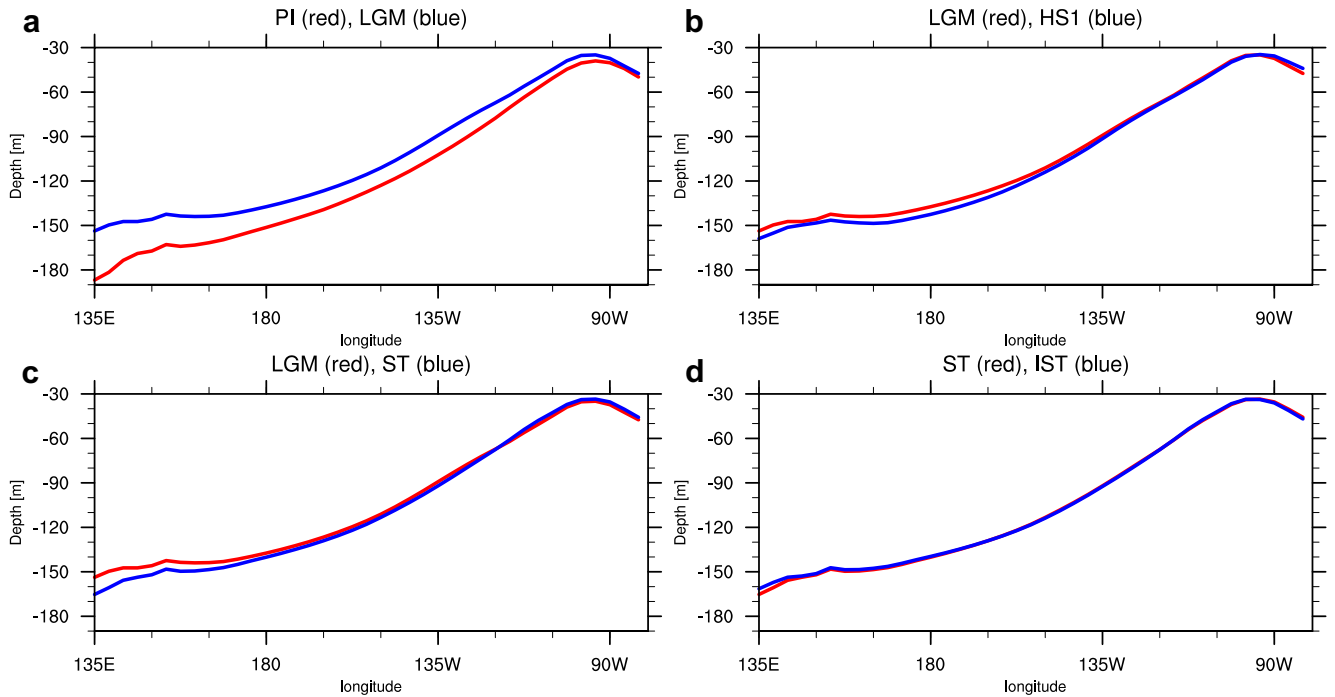


Fig. 7. Annual mean depth of the 17°C isotherm along the equator for a) PI and LGM, b) LGM and HS1, c) LGM and ST, d) ST and IST. Shown are latitudinal averages for 5°S–5°N. Units: m.

thermocline depth responses in the IST experiment (w.r.t. ST) are an order of magnitude smaller than in the other experiments (Figs. 8d and 10d).

According to Cessi et al. (2004) and Timmermann et al. (2005) a shutdown of the North Atlantic meridional overturning leads to a deepening of the tropical Pacific thermocline a few decades later and to a subsequent weakening of ENSO variability through

a less efficient thermocline feedback (Zebiak and Cane, 1987). Interestingly, Yeh et al. (2009) described a shallowing in the tropical thermocline and enhanced ENSO variability for future climate changes. This would be consistent with a more efficient thermocline feedback according to Fedorov and Philander (2001) who find that a shallower zonal mean thermocline leads to enhanced ENSO variability. In contrast, our HS1 results suggest an

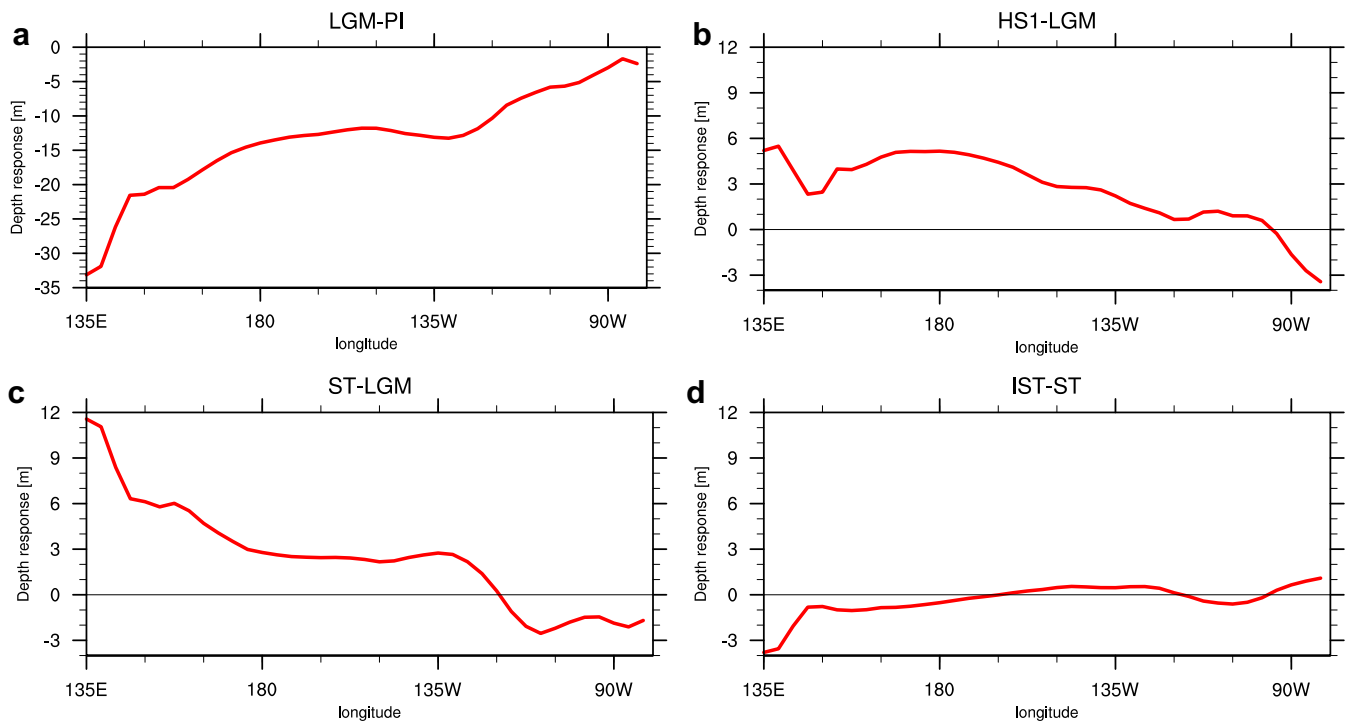


Fig. 8. As Fig. 7, but showing the response between the respective two experiments. Positive values in the response of thermocline depth correspond to a deepening.

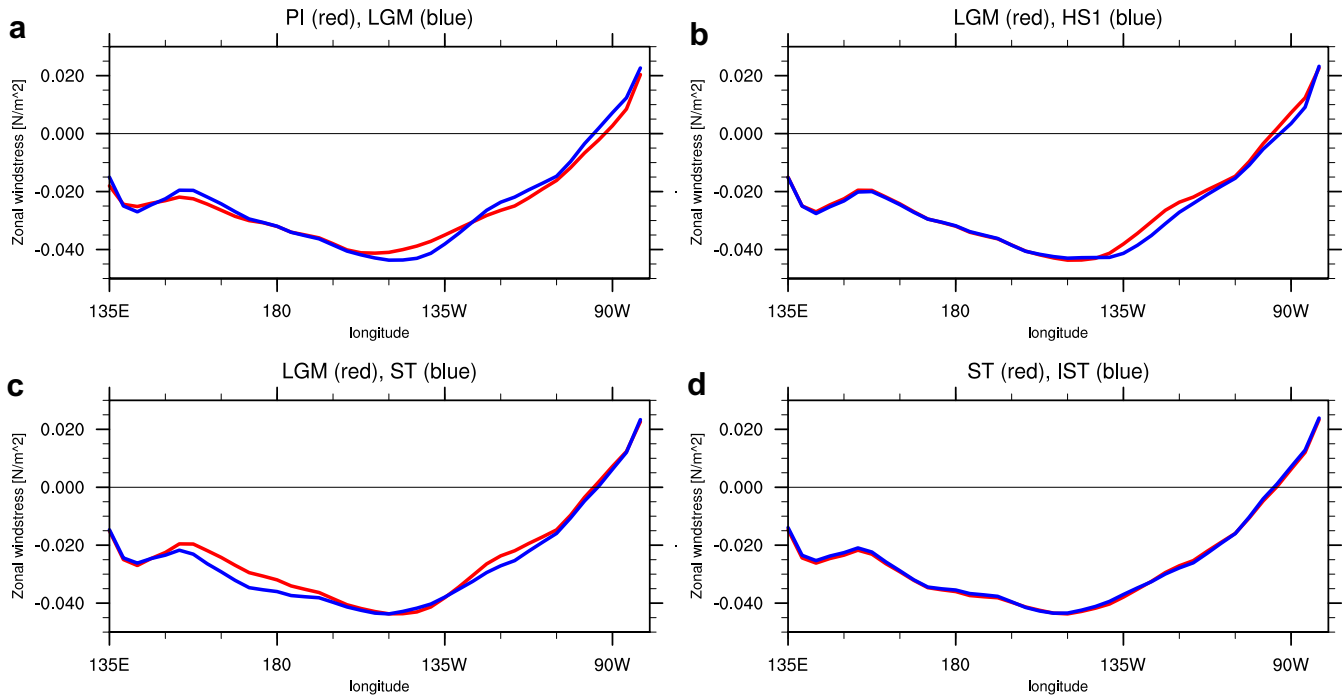


Fig. 9. Annual mean zonal wind stress along the equator for a) PI and LGM, b) LGM and HS1, c) LGM and ST, d) ST and IST. Shown are latitudinal averages for 5°S–5°N. Units: Nm^{-2} .

increase of ENSO variability in spite of an overall deepening of the thermocline, similar to the results by Matei et al. (2008) who also find an ENSO enhancement with a mean deepening of the tropical Pacific thermocline. Therefore, we attribute our simulated HS1 increase of ENSO variability to an atmospheric bridge from the Atlantic to the Pacific via trade wind forcing, to a subsequent modification of the annual cycle and to a steepening of the thermocline.

5. ENSO teleconnections

With respect to the considerable reorganization of atmospheric dynamics during glacial times (Kageyama et al., 1999; Justino et al., 2005), it is worthwhile to also investigate how ENSO teleconnections were affected by the different glacial boundary conditions. In order to identify ENSO teleconnections, we performed a composite analysis of different climate parameters. Here,

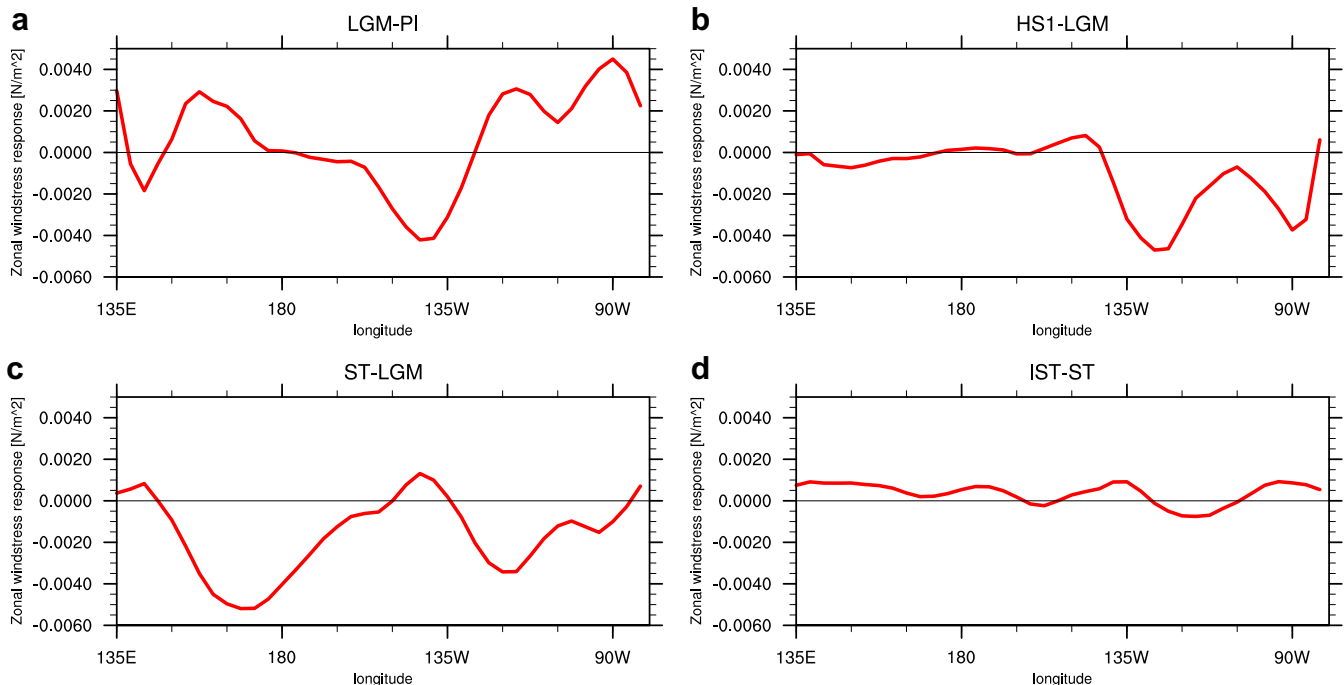


Fig. 10. As Fig. 9, but showing the response between the respective two experiments.

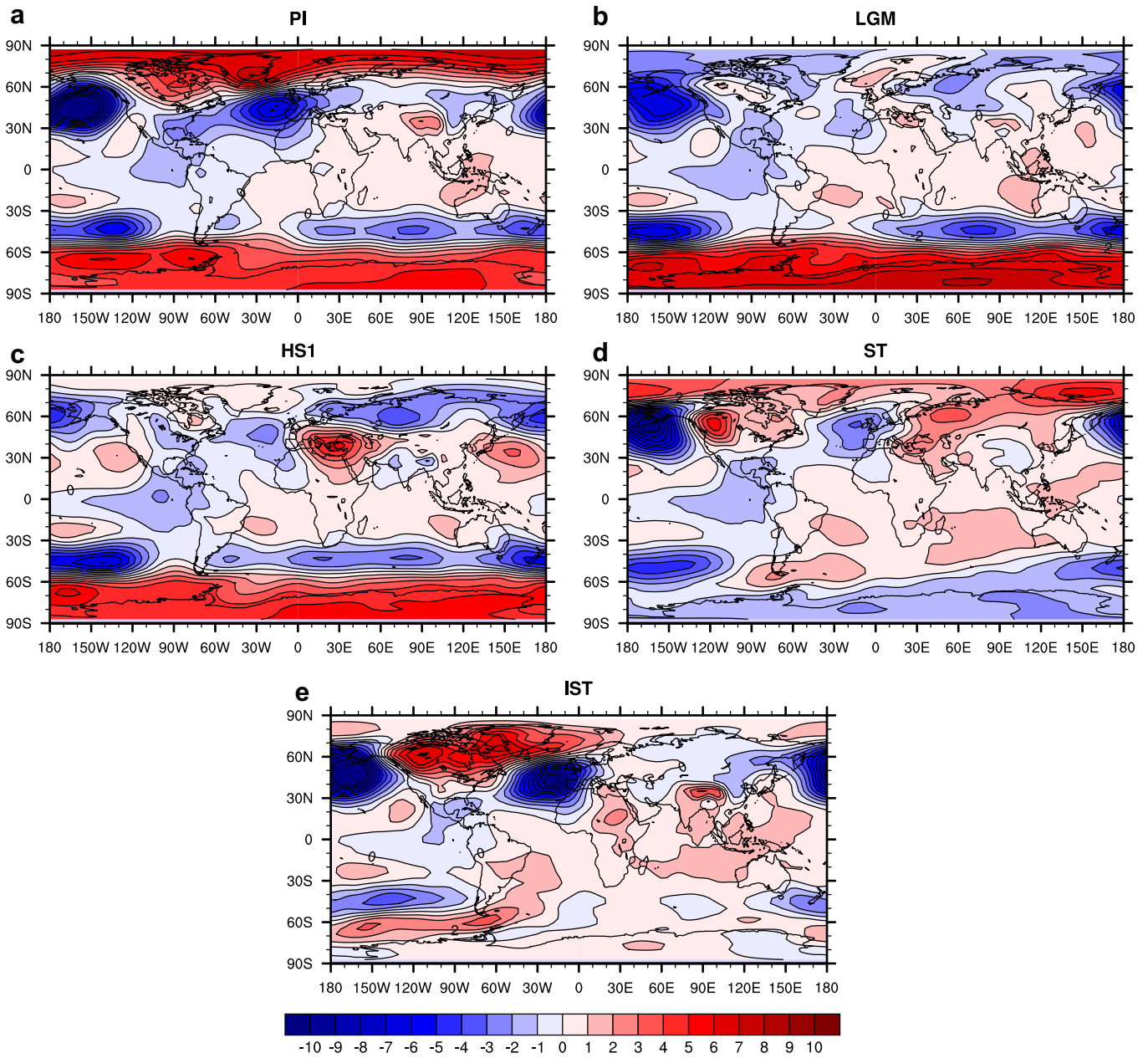


Fig. 11. Boreal winter (DJF) ENSO teleconnections of sea-level pressure shown as differences between the El Niño composite and the La Niña composite for a) preindustrial control, b) LGM, c) Heinrich Stadial 1, d) stadial, and e) interstadial simulations. Units are hPa.

we focus on the boreal winter season (December–February, DJF). This is motivated by the observational evidence of El Niño peaking during boreal winter and by the fact that ENSO teleconnections tend to be most pronounced during this season (Horel and Wallace, 1981). Seasonal mean anomalies with respect to the long-term mean climatology are computed and composited into El Niño and La Niña events. The identification of El Niño and La Niña seasons contributing to the composites is based on the threshold criterion that the seasonal mean Niño3 SST index exceeds one standard deviation (El Niño) or falls below minus one standard deviation (La Niña), respectively. Averaging over the events falling into each of the two categories determines the characteristic responses to El Niño and La Niña. Composite analysis is based on the assumption of a linear response of the atmosphere to ENSO events, i.e. the response to La Niña events is assumed to exhibit

the same pattern as the response to El Niño events but with opposite polarity. We follow this approach to investigate the first-order response to glacial boundary conditions and will address the nonlinearity of teleconnections (DeWeaver and Nigam, 2002) in an ongoing study. Results from the composite analysis are shown as differences between El Niño composites and La Niña composites for each experiment (Figs. 11–14).

For the PI simulation, the well-known intensification of the Aleutian low forced by El Niño is clearly evident as well as a Pacific/North America pattern (PNA)-like multipole structure of sea-level pressure anomalies over the North Pacific and North America (Fig. 11a). Downstream of the North American continent, sea-level pressure anomalies exhibit a meridional dipole-like structure reflecting the negative phase of the North Atlantic Oscillation (NAO). Such a teleconnection has been observed (Huang et al.,

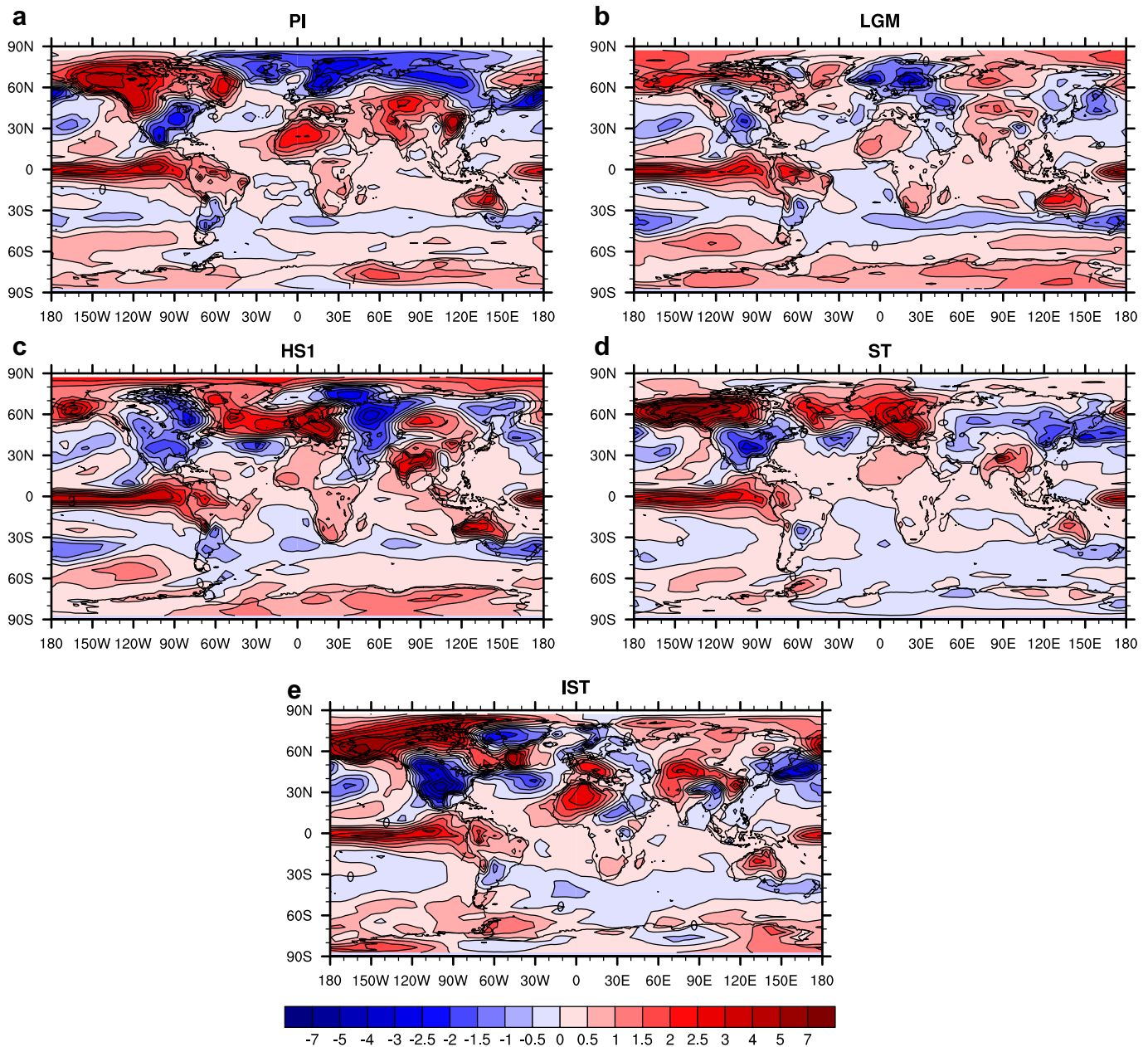


Fig. 12. As Fig. 11, but for surface temperature. Units are K. Note the irregular contour intervals.

1998) and is overestimated by the CCSM3 model (for a comparison with observations see Deser et al., 2006). For the LGM (Fig. 11b), the model simulates the strongest changes in the ENSO teleconnections over North America and the North Atlantic. These changes must be related to the presence of the Laurentide ice sheet blocking the usual Rossby-wave like signal communication to the extratropics. The dipole over the North Atlantic completely vanishes under LGM and HS1 conditions (Fig. 11b,c). For the latter, also the El Niño-related pattern over the North Pacific Ocean breaks down and the intensification of the Aleutian Low is even less pronounced than in the LGM simulation. The large-scale pattern of the ENSO teleconnections to the Southern Hemisphere is rather similar in our PI, LGM and HS1 simulations during boreal winter. For austral winter seasons, the teleconnections are discussed in more detail in Timmermann et al. (2010). Interestingly, the atmospheric bridge from the tropical Pacific over the North American continent into the

North Atlantic area reappears in our ST and IST simulations which are both characterized by considerably lower continental ice sheet topography which reduces the barrier to atmospheric Rossby-wave propagation. The location of the nodal line over the North Atlantic, however, is different between ST and IST experiments (Fig. 11d,e) with important implications for the predominant wind field and the associated sea-ice export from the Arctic.

A strong dependency of the ENSO-related anomalies on the climatic background state is also found for surface temperature (Fig. 12). By construction, the eastern tropical Pacific warming along the equator during El Niño events is evident in all simulations. The extratropical part of the composite difference, however, shows a remarkably different structure and amplitude in the different experiments. In the PI run, anomalies concomitant with the intensification of the Aleutian Low lead to a pronounced warming (cooling) over the North American continent during El

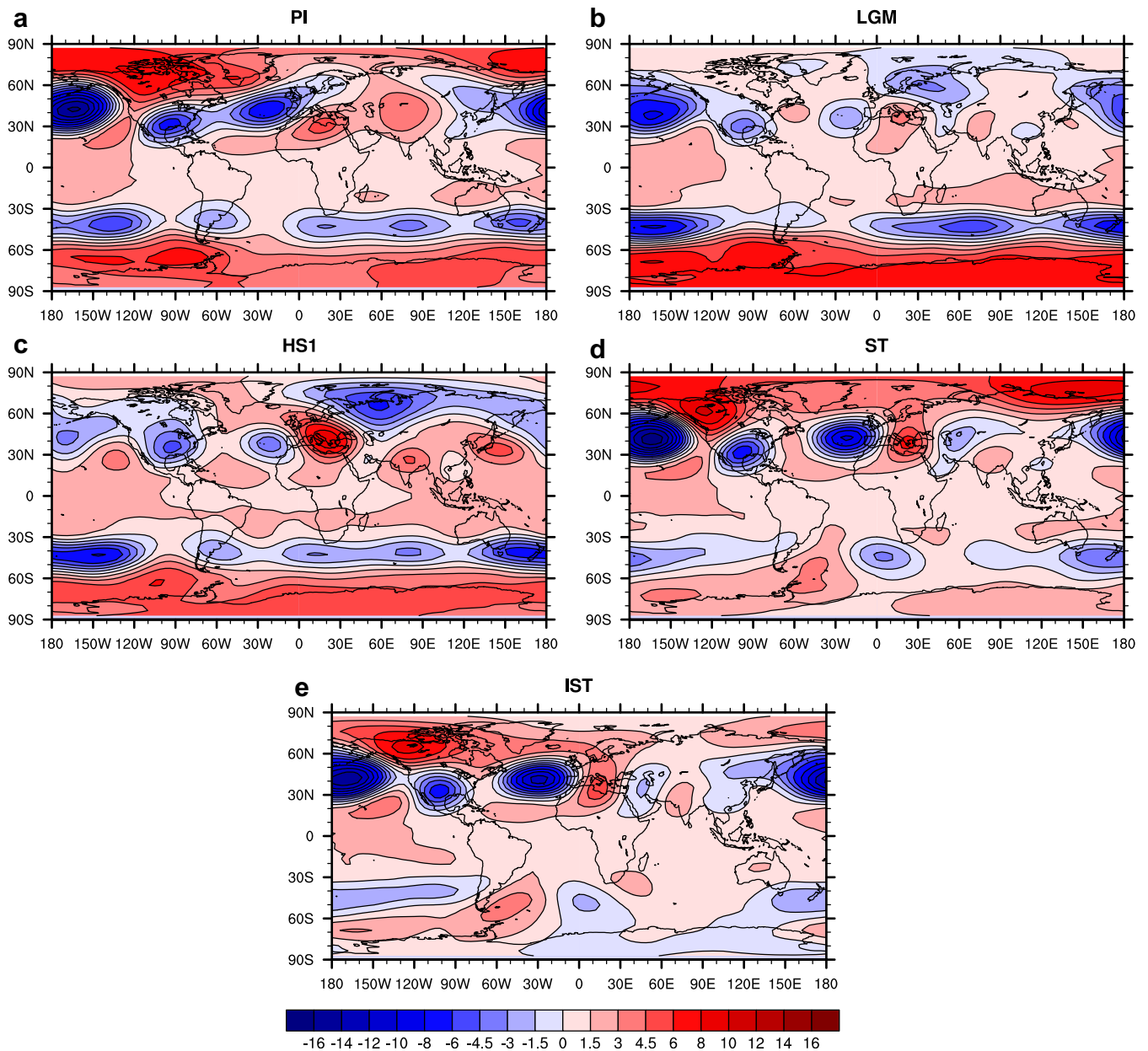


Fig. 13. As Fig. 11, but for 500 hPa geopotential height. Units are gpm. Note the irregular contour intervals.

Niño (La Niña). This pattern vanishes completely in the LGM run and even reverses its polarity in the HS1 simulation. Since the prescribed Laurentide ice sheet is the same in the LGM and HS1 simulations, the difference between the two patterns is due to the extratropical bridge between the North Atlantic and North Pacific regions being modified by the cooling over the North Atlantic associated with the strong AMOC weakening. ENSO composite differences resemble the PI pattern for the stadial and interstadial experiments over the North Pacific and North America (Fig. 12d,e). However, over the North Atlantic/European sector, 35 ka simulations are different from PI suggesting a modulation of the teleconnections by the presence of the 35 ka ice sheet. El Niño cooling over central and southern North America is strongest in the IST run (Fig. 12e). Both PI and IST experiments show a strong signal over northwest Africa. The warming (cooling) over Australia during El Niño (La Niña) remains remarkably stable throughout the different experiments.

ENSO teleconnections typically involve a dynamical reorganization also of the middle and upper troposphere. Therefore, ENSO-related anomalies in 500 hPa geopotential height are shown for the different climatic states in Fig. 13. The PI simulation exhibits a PNA-like structure over the North Pacific/North America and also shows the well-pronounced Aleutian low already seen in Fig. 11. With LGM boundary conditions (Fig. 13b), the wavetrain emanating from the tropical Pacific is deviated to the south of the Laurentide ice sheet and seems confined to the subtropics. In HS1 (Fig. 13c), a similar wavetrain of geopotential height anomalies is found together with a more pronounced ENSO signature over the eastern North Atlantic/European sector compared to the LGM. This could result from an amplification of the wavetrain by the negative North Atlantic SST anomalies at HS1 which would be consistent with a high-pressure anomaly downstream of negative SSTA (e.g. Palmer and Sun, 1985). Comparison with HS1 sea-level pressure composite (Fig. 11c) reveals the equivalent-barotropic nature of the anomalies

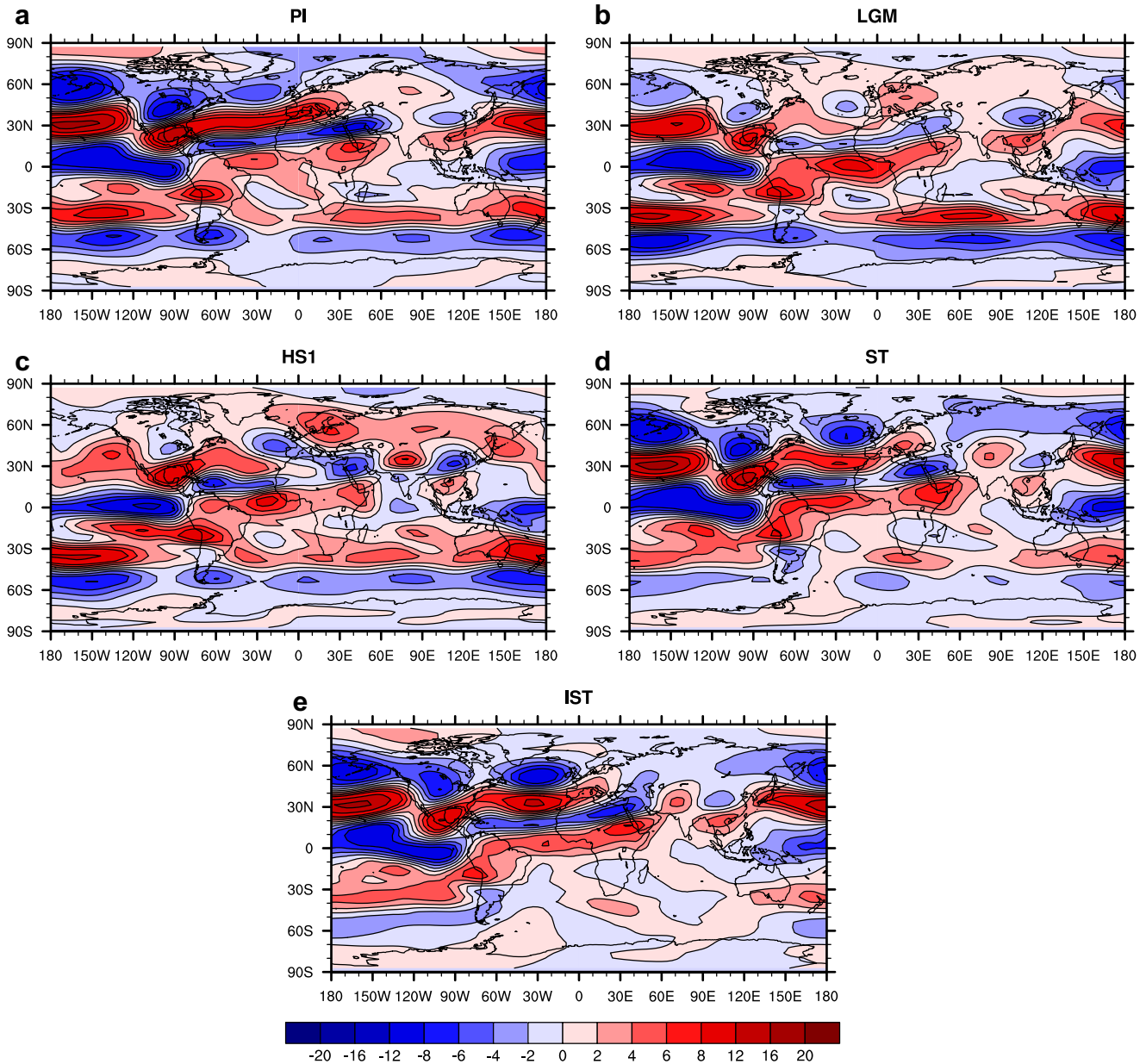


Fig. 14. As Fig. 11, but for 200 hPa zonal wind. Units are m/s. Note the irregular contour intervals.

over the North Atlantic/European sector. Interestingly, the 500 hPa ENSO teleconnections for ST and IST look extremely similar. This suggests that the weak freshwater extraction in IST – the only difference between ST and IST – does not impact on mid-tropospheric dynamics compared to ST, but only allows a near-surface modulation of ENSO impacts in the North Atlantic/European sector (Figs. 11 and 13d,e).

At the jetstream level at 200 hPa height, the global-scale nature of ENSO teleconnections becomes evident from pronounced anomalies of zonal wind speed. It can be seen that the upper branch of the Walker circulation is weakened over the tropical Pacific and that the subtropical jetstream is intensified over the North Pacific/North American continent and well extended into the North Atlantic sector at all climatic states (Fig. 14). However, for the LGM and HS1, the whole pattern seems to be shifted southward with a clearly reduced ENSO impact over northern North America and the North Atlantic which could be due to the influence of the Laurentide ice sheet which induces a splitting and deviation of the

jet towards the north and the south of the continental ice “obstacle”. ST and IST show strong structural similarities in the 200 hPa zonal wind composite pattern (Fig. 14d,e). A robust attribution whether this similarity within the MIS3 experiments is due to a compensation of the impact of the various 35 ka BP forcings on ENSO teleconnections would require further sensitivity experiments isolating the individual influence of either of the boundary forcings in analogy to Yin and Battisti (2001).

So far, we focussed on the teleconnections to the Northern Hemisphere during boreal winter season (DJF). Glacial tropical-extra-tropical teleconnections to the Southern Hemisphere during austral winter season (JJA), however, are also of great relevance. Preliminary results from the austral winter season (June–August, JJA) confirm our findings presented here. Timmermann et al. (2010) demonstrated that these teleconnections to the Southern Hemisphere need to be studied more closely in order to elucidate discrepancies between warming trends shown by different Antarctic ice core records.

Recalling the changes in ENSO variability discussed before, it is important to note that ENSO teleconnections can be modified even if there is no major change in tropical Pacific variability. With glacial boundary conditions in particular, it appears that the tropical-extratropical signal communication works as under modern conditions, but that the mid-latitude atmospheric dynamics is strongly modified by the topography forcing associated with the Laurentide and Fennoscandian ice sheets.

6. Conclusions

We have presented results from a set of experiments for the Last Glacial Maximum and Marine Isotope Stage 3 using the CCSM3 model. The goal of this paper was to study tropical Pacific variability and the associated ENSO teleconnections for different glacial climates designed to mimic the Last Glacial Maximum, Heinrich Stadial 1, and a Dansgaard-Oeschger stadial and interstadial.

One of the most remarkable results of our study is the strong dependence of ENSO teleconnections on the respective background climatic state. This demonstrates that ENSO teleconnections respond to climate changes even if tropical Pacific variability does not change significantly compared to the preindustrial reference state. An exception to this is found in our Heinrich Stadial 1 simulation. Here, ENSO teleconnections are influenced not only by the glacial boundary conditions and a weakening of the Atlantic Ocean meridional overturning circulation, but also by increased tropical Pacific variability.

In the context of orbital-scale and abrupt climate variations, it is important to note the cause-and-effect as well as the two-way problems inherent to tropical-extratropical signal communication. On the one hand, the response of the tropical climate system to various kinds of forcings (such as orbital forcing, greenhouse gas concentrations) needs to be understood. A first effort to test the relationship between orbital forcing and ENSO variability has been presented by Timmermann et al. (2007a) who applied an acceleration method to the ECHAM4-HOPE model and largely confirmed the Clement et al. (1999) hypothesis of an orbital impact of ENSO variability. However, no other boundary conditions such as time-varying greenhouse gas concentrations or continental ice sheet topography have been taken into account in that study. Our results demonstrate that in addition to orbital forcing, other factors such as greenhouse gas concentrations or high-latitude freshwater perturbations contribute to the non-stationarity of tropical Pacific climate in different climatic states. In turn, changes in ENSO variability may induce abrupt changes in high latitudes. However, in order to robustly test the Cane and Clement (1999) hypothesis on a tropical triggering of abrupt climate change, e.g. the build-up or melting of high-latitude ice sheets, long simulations with comprehensive general circulation models including a continental ice sheet model would be required. In our setup, no statements about the interaction of the Laurentide ice sheet, for instance, with forcing from the tropics are possible. However, we can conclude that despite ENSO variability being active at glacial periods, ENSO teleconnections to the extratropics are not stationary. Accordingly, past orbital and millennial-scale climate variability should only be discussed with caution in terms of present-day climate modes and teleconnections. Specifically, our results challenge the hypothesis of Clement and Cane (1999) with respect to its underlying assumption of stationary ENSO teleconnections.

Acknowledgments

This work has received funding from the research project SCHU1389/6-1 of the Deutsche Forschungsgemeinschaft (DFG) and through the DFG-Research Center/Excellence Cluster “The Ocean in

the Earth System”. We gratefully acknowledge the advice by Bruce Briegleb, Ian Eisenman, and Jaqueline Flückiger for setting up our CCSM3 simulations. The simulations have all been performed on the IBM supercomputer of the Norddeutscher Verbund für Hoch- und Höchstleistungsrechnen (HLRN) in Hannover, Germany.

References

- Ahn, J., Brook, E.J., 2007. Atmospheric CO₂ and climate from 65 to 30 ka B.P. *Geophys. Res. Lett.* 34, L10703. doi:10.1029/2007GL029551.
- Arz, H.W., Lamy, F., Ganopolski, A., Nowaczyk, N., Pätzold, J., 2007. Dominant northern hemisphere climate control over millennial-scale glacial sea-level variability. *Quat. Sci. Rev.* 26, 312–321.
- Barron, E., Pollard, D., 2002. High-resolution climate simulations of Oxygen Isotope Stage 3 in Europe. *Quat. Res.* 58, 296–309.
- Bitz, C.M., Chiang, J.C.H., Cheng, W., Barsugli, J.J., 2007. Rates of thermohaline recovery from freshwater pulses in modern, Last Glacial Maximum, and greenhouse warming climates. *Geophys. Res. Lett.* 34, L07708. doi:10.1029/2006GL029237.
- Braconnot, P., Otto-Bliesner, B., Harrison, S., Joussaume, S., Peterschmitt, J.-Y., Abe-Ouchi, A., Crucifix, M., Driesschaert, E., Fichefet, Th., Hewitt, C.D., Kageyama, M., Kitoh, A., Laine, A., Marti, O., Merkel, U., Ramstein, G., Valdes, P., Weber, S.L., Yu, Y., Zhao, Y., 2007a. Results of PMIP2 coupled simulations of the Mid-Holocene and Last Glacial maximum – Part 1: experiments and large-scale features. *Clim. Past* 3, 261–277.
- Braconnot, P., Otto-Bliesner, B., Harrison, S., Joussaume, S., Peterschmitt, J.-Y., Abe-Ouchi, A., Crucifix, M., Driesschaert, E., Fichefet, Th., Hewitt, C.D., Kageyama, M., Kitoh, A., Loutre, M.-F., Marti, O., Merkel, U., Ramstein, G., Valdes, P., Weber, S.L., Yu, Y., Zhao, Y., 2007b. Results of PMIP2 coupled simulations of the Mid-Holocene and Last Glacial maximum – Part 2: feedbacks with emphasis on the location of the ITCZ and mid- and high latitudes heat budget. *Clim. Past* 3, 279–296.
- Burgers, G., Stephenson, D.B., 1999. The “Normality” of El Niño. *Geophys. Res. Lett.* 26 (No. 8), 1027–1030.
- Cane, M.A., Clement, A.C., 1999. A role for the tropical Pacific coupled ocean-atmosphere system on Milankovitch and Millennial timescales. Part II: global impacts. *AGU Geophysical Monograph Series*, 112. In: Clark, P.U., Webb, R.S., Keigwin, L.D. (Eds.), *Mechanisms of global climate change at Millennial timescales*, pp. 373–383.
- Cessi, P., Bryan, K., Zhang, R., 2004. Global seiching of thermocline waters between the Atlantic and the Indian-Pacific Ocean Basins. *Geophys. Res. Lett.* 31, L04302. doi:10.1029/2003GL019091.
- Chappell, J., 2002. Sea level changes forced ice breakouts in the Last Glacial cycle: new results from coral terraces. *Quat. Sci. Rev.* 21 (10), 1229–1240.
- Clement, A.C., Cane, M.A., 1999. A role for the tropical Pacific coupled ocean-atmosphere system on Milankovitch and millennial timescales. Part I: a modeling study of tropical Pacific variability. *AGU Geophysical Monograph Series*, 112. In: Clark, P.U., Webb, R.S., Keigwin, L.D. (Eds.), *Mechanisms of global climate change at Millennial timescales*, pp. 363–372.
- Clement, A.C., Peterson, L.C., 2008. Mechanisms of abrupt climate change of the Last Glacial Period. *Rev. Geophys.* 46, RG4002. doi:10.1029/2006RG000204.
- Clement, A.C., Seager, R., Cane, M.A., 1999. Orbital controls on the El Niño/Southern Oscillation and the tropical climate. *Paleoceanography* 14 (No. 4), 441–456.
- Collins, M., the CMIP Modelling Groups, 2005. El Niño- or La Niña-like climate change? *Clim. Dynamics* 24, 89–104. doi:10.1007/s00382-004-0478-x.
- Collins, W.D., Bitz, C.M., Blackmon, M.L., Bonan, G.B., Bretherton, C.S., Carton, J.A., Chang, P., Doney, S.C., Hack, J.J., Henderson, T.B., Kiehl, J.T., Large, W.G., McKenna, D.S., Santer, B.D., Smith, R.D., 2006. The community climate system model version (CCSM3). *J. Clim.* 19, 2122–2143.
- Deser, C., Capotondi, A., Saravanan, R., Philipps, A.S., 2006. Tropical Pacific and Atlantic Climate variability in CCSM3. *J. Clim.* 19, 2451–2481.
- DeWeaver, E., Nigam, S., 2002. Linearity in ENSO's atmospheric response. *J. Clim.* 15 (No. 17), 2446–2461.
- Dommengat, D., Stammer, D., 2004. Assessing ENSO simulations and predictions using adjoint ocean state estimation. *J. Clim.* 17 (No. 22), 4301–4315.
- Eisenman, I., 2008. Abrupt climate change: North Atlantic volatility during the last ice age and modern Arctic sea ice retreat. PhD thesis, Harvard University.
- Fedorov, A.V., Philander, S.G., 2001. A stability analysis of tropical ocean-atmosphere interaction: bridging measurements and theory for El Niño. *J. Clim.* 14, 3086–3101.
- Flückiger, J., Blunier, T., Stauffer, B., Chappellaz, J., Spahni, R., Kawamura, K., Schwander, J., Stocker, T.F., Dahl-Jensen, D., 2004. N₂O and CH₄ variations during the last glacial epoch: insight into global processes. *Global Biogeochem. Cycles* 18, GB1020. doi:10.1029/2003GB002122.
- Guilyardi, E., 2006. El Niño-mean state-seasonal cycle interactions in a multi-model ensemble. *Clim. Dynamics* 26, 329–348. doi:10.1007/s00382-005-0084-6.
- Guilyardi, E., Wittenberg, A., Fedorov, A., Collins, M., Wang, C., Capotondi, A., van Oldenborgh, G.-J., Stockdale, T., 2009. Understanding El Niño in Ocean-Atmosphere General Circulation Models – progress and challenges. *B. Am. Meteorol. Soc.* 90 (No. 3), 325–340.
- Horel, J.D., Wallace, J.M., 1981. Planetary-scale atmospheric phenomena associated with the Southern Oscillation. *Mon. Wea. Rev.* 109, 1–6. No. 4, 813–829.

- Hu, A., Otto-Bliessner, B., Meehl, G., Han, W., Morrill, C., Brady, E., Briegleb, B., 2008. Response of thermohaline circulation to freshwater forcing under present-day and LGM conditions. *J. Clim.* 21, 2239–2258.
- Huang, J., Higuchi, K., Shabbar, A., 1998. The relationship between the North Atlantic Oscillation and the El Niño–Southern Oscillation. *Geophys. Res. Lett.* 25 (14), 2707–2710.
- Huang, R., Cane, M., Naik, N., Goodman, P., 2000. Global adjustment of the thermocline in response to deepwater formation. *Geophys. Res. Lett.* 27, 759–762.
- Jin, F.-F., An, S.-I., 1999. Thermocline and zonal advective feedbacks within the equatorial ocean recharge oscillator model for ENSO. *Geophys. Res. Lett.* 26 (19), 2989–2992.
- Jin, F.-F., Neelin, J.D., Ghil, M., April 1994. El Niño on the devil's staircase: annual subharmonic steps to chaos. *Science* 264 (1), 70–72.
- Jin, L., Chen, F., Ganopolski, A., Claussen, M., 2007. Response of East Asian climate to Dansgaard/Oeschger and Heinrich events in a coupled model of intermediate climate complexity. *J. Geophys. Res.* 112, D06117. doi:10.1029/2006JD007316.
- Justino, F., Timmermann, A., Merkel, U., Souza, E.P., 2005. Synoptic reorganization of atmospheric flow during the Last Glacial Maximum. *J. Clim.* 18, 2826–2846.
- Kageyama, M., Valdes, P.J., Ramstein, G., Hewitt, C., Wyputta, U., 1999. northern hemisphere storm tracks in present day and Last Glacial Maximum climate simulations: a comparison of the European PMIP models. *J. Clim.* 12, 742–760.
- Koutavas, A., Lynch-Stieglitz, J., Marchitto Jr., T.M., Sachs, J.P., 2002. El Niño-like pattern in ice age tropical Pacific sea surface temperature. *Science* 297, 226–230.
- Lañé, A., Kageyama, M., Salas-Mélia, D., Voltaire, A., Rivière, G., Ramstein, G., Planton, S., Tyteca, S., Peterschmitt, J.-Y., 2008. Northern hemisphere storm tracks during the Last Glacial Maximum in the PMIP2 Ocean–Atmosphere coupled models: energetic study, seasonal cycle, precipitation. *Clim. Dynamics* published online 04/11/2008.
- Latif, M., Anderson, D., Barnett, T., Cane, M., Kleeman, R., Leetma, A., O'Brien, J., Rosati, A., Schneider, E., 1998. A review of the predictability and prediction of ENSO. *J. Geophys. Res.* 103 (C7), 14,375–14,393.
- Liu, Z., 2002. A simple model study of the forced response of ENSO to an external periodic forcing. *J. Clim.* 15, 1088–1098.
- Lynch-Stieglitz, J., Adkins, J.F., Curry, W.B., Dokken, T., Hall, I.R., Herguera, J.C., Hirschi, J., Ivanova, E.V., Kissel, C., Marchal, O., Marchitto, T.M., McCave, I.N., McManus, J.F., Mulitza, S., Ninnemann, U., Peeters, F., Yu, E.-F., Zahn, R., 2007. Atlantic meridional overturning circulation during the Last Glacial Maximum. *Science* 316, 66–69.
- Matei, D., Keenlyside, N.S., Latif, M., Jungclauss, J., 2008. Subtropical forcing of tropical Pacific climate and decadal ENSO modulation. *J. Clim.* 21, 4691–4709.
- McManus, J.F., Francois, R., Gherardi, J.-M., Keigwin, L.D., Brown-Leger, S., 2004. Collapse and rapid resumption of Atlantic meridional circulation linked to deglacial climate changes. *Nature* 428, 834–837.
- Merryfield, W.J., 2006. Changes to ENSO under CO₂ doubling in a multimodel ensemble. *J. Clim.* 19, 4009–4027.
- Müller, W., Roeckner, E., 2008. ENSO teleconnections in projections of future climate in ECHAM5/MPI-OM. *Clim. Dynamics* 31, 533–549. doi:10.1007/s00382-007-0357-3.
- Otto-Bliessner, B.L., Brady, E.C., Shin, S.-I., Liu, Z., Shields, C., 2003. Modeling El Niño and its tropical teleconnections during the last glacial-interglacial cycle. *Geophys. Res. Lett.* 30 (23), 2198. doi:10.1029/2003GL018553.
- Otto-Bliessner, B.L., Brady, E.C., Clauzet, G., Tomas, R., Levis, S., Kothavala, Z., 2006a. Last glacial maximum and Holocene climate in CCSM3. *J. Clim.* 19, 2526–2544.
- Otto-Bliessner, B.L., Tomas, R., Brady, E.C., Ammann, C., Kothavala, Z., Clauzet, G., 2006b. Climate sensitivity of moderate- and low-resolution versions of CCSM3 to preindustrial forcings. *J. Clim.* 19, 2567–2583.
- Palmer, T.N., Sun, Z., 1985. A modelling and observational study of the relationship between sea surface temperature in the north-west Atlantic and the atmospheric general circulation. *Quart. J. Roy. Meteor. Soc.* 111, 947–975.
- Peltier, W.R., 2004. Global glacial isostasy and the surface of the ice-age Earth: the ICE-5G (VM2) model and GRACE. *Annu. Rev. Earth Planet. Sci.* 32, 111–149.
- Peltier, W.R., Solheim, L.P., 2004. The climate of the Earth at Last Glacial Maximum: statistical equilibrium state and a mode of internal variability. *Quat. Sci. Rev.* 23, 335–357.
- Pena, L.D., Cacho, I., Ferretti, P., Hall, M.A., 2008. El Niño–Southern Oscillation-like variability during glacial terminations and interlatitudinal teleconnections. *Paleoceanography* 23, PA3101. doi:10.1029/2008PA001620.
- Rein, B., Lückge, A., Reinhardt, L., Sirocko, F., Wolf, A., Dullo, W.-C., 2005. El Niño variability off Peru during the last 20,000 years. *Paleoceanography* 20, PA4003. doi:10.1029/2004PA001099.
- Rohling, E.J., Grant, K., Hemleben, C., Kucera, M., Roberts, A.P., Schmeltzer, I., Schulz, H., Siccha, M., Siddall, M., Trommer, G., 2008. New constraints on the timing of sea level fluctuations during early to middle marine isotope stage 3. *Paleoceanography* 23, PA3219. doi:10.1029/2008PA001617.
- Sarnthein, M., Statterger, K., Dreger, D., Erlenkeuser, H., Grootes, P., Haupt, B.J., Jung, S., Kiefer, T., Kuhnt, W., Pflaumann, U., Schäfer-Neth, C., Schulz, H., Schulz, M., Seidov, D., Simstich, J., van Kreveld, S., Vogelsang, E., Völker, A., Weinelt, M., 2001. Fundamental modes and abrupt changes in the North Atlantic circulation and climate over the last 60 Ky – concepts, reconstructions and numerical modeling. In: Schäfer, P., Ritzrau, W., Schlüter, M., Thiede, J. (Eds.), *The Northern North Atlantic: a changing environment*. Springer, Berlin, pp. 365–410.
- Siddall, M., Rohling, E.J., Almogi-Labin, A., Hemleben, Ch., Meischner, D., Schmelzer, I., Smeed, D.A., 2003. Sea-level fluctuations during the last glacial cycle. *Nature* 423, 853–858.
- Siddall, M., Rohling, E.J., Thompson, W.G., Waelbroeck, C., 2008. Marine Isotope Stage 3 sea level fluctuations: data synthesis and new outlook. *Rev. Geophys.* 46, RG4003. doi:10.1029/2007RG000226.
- Spahni, R., Chappellaz, J., Stocker, T.F., Loulergue, L., Hausammann, G., Kawamura, K., Flückiger, J., Schwander, J., Raynaud, D., Masson-Delmotte, V., Jouzel, J., 2005. Atmospheric methane and nitrous oxide of the Late Pleistocene from Antarctic ice cores. *Science* 310, 1317–1321.
- Stott, L., Poulsen, C., Lund, S., Thunell, R., 2002. Super ENSO and global climate oscillations at millennial time scales. *Science* 297, 222–226.
- Stouffer, R.J., Yin, J., Gregory, J.M., Dixon, K.W., Spelman, M.J., Hurlin, W., Weaver, A.J., Eby, M., Flato, G.M., Hasumi, H., Hu, A., Jungclauss, J.H., Kamenkovich, I.V., Levermann, A., Montoya, M., Murakami, S., Nawrath, S., Oka, A., Peltier, W.R., Robitaille, D.Y., Sokolov, A., Vettoretti, G., Weber, S.L., 2006. Investigating the causes of the response of the thermohaline circulation to past and future climate changes. *J. Clim.* 19, 1365–1387.
- Timmermann, A., Oberhuber, J., Bacher, A., Esch, M., Latif, M., Roeckner, E., 1999. Increased El Niño frequency in a climate model forced by future greenhouse warming. *Nature* 398, 694–697.
- Timmermann, A., An, S.-I., Krebs, U., Goosse, H., 2005. ENSO suppression due to weakening of the North Atlantic thermohaline circulation. *J. Clim.* 18, 3122–3139.
- Timmermann, A., Lorenz, S.J., An, S.-I., Clement, A., Xie, S.-P., 2007a. The effect of orbital forcing on the mean climate and variability of the tropical Pacific. *J. Clim.* 20, 4147–4159.
- Timmermann, A., Okumura, Y., An, S.-I., Clement, A., Dong, B., Guilyardi, E., Hu, A., Jungclauss, J.H., Renold, M., Stocker, T.F., Stouffer, R.J., Sutton, R., Xie, S.-P., Yin, J., 2007b. The influence of a weakening of the Atlantic Meridional overturning Circulation on ENSO. *J. Clim.* 20, 4899–4919.
- Timmermann, A., Menviel, L., Okumura, Y., Schilla, A., Merkel, U., Timm, O., Hu, A., Schulz, M., 2010. Towards a quantitative understanding of millennial-scale Antarctic Warming Events. *Quat. Sci. Rev. EPICA special Issue*, 29, 74–85.
- Trenberth, K.E., 1997. The definition of El Niño. *Bull. Am. Meteor. Soc.* 78, 2771–2777.
- Tudhope, A.W., Chilcott, C.P., McCulloch, M.T., Cook, E.R., Chappell, J., Ellam, R.M., Lea, D.W., Lough, J.M., Shimmield, G.B., 2001. Variability in the El Niño–Southern oscillation during a glacial-interglacial cycle. *Science* 291, 1511–1517.
- Tziperman, E., Stone, L., Cane, M.A., Jarosh, H., 1994. El Niño chaos: overlapping of resonances between the seasonal cycle and the Pacific Ocean–Atmosphere oscillator. *Science* 264, 72–74.
- van Meerbeeck, C.J., Renssen, H., Roche, D.M., 2009. How die Marine Isotope Stage 3 and Last Glacial maximum climates differ? Perspectives from equilibrium simulations. *Clim. Past* 5, 33–51.
- van Oldenborgh, G.J., Philip, S.Y., Collins, M., 2005. El Niño in a changing climate: a multi-model study. *Ocean Sci.* 1, 81–95.
- Xie, S.-P., 1994. On the genesis of the equatorial annual cycle. *J. Clim.* 7, 2008–2013.
- Yeager, S.G., Shields, C.A., Large, W.G., Hack, J.J., 2006. The low-resolution CCSM3. *J. Clim.* 19, 2545–2566.
- Yeh, S.-W., Kug, J.-S., Dewitte, B., Kwon, M.-H., Kirtman, B.P., Jin, F.-F., 2009. El Niño in a changing climate. *Nature* 461. doi:10.1038/nature08316.
- Yin, J.H., Battisti, D.S., 2001. The importance of tropical sea surface temperature patterns in simulations of last glacial maximum climate. *J. Clim.* 14, 565–581.
- Zebiak, S.E., Cane, M.A., 1987. A Model El Niño–Southern Oscillation. *Mon. Wea. Rev.* 115, 2262–2278.
- Zhang, R., Delworth, T.L., 2005. Simulated tropical response to a substantial weakening of the Atlantic thermohaline circulation. *J. Clim.* 18, 1853–1860.
- Zheng, W., Braconnot, P., Guilyardi, E., Merkel, U., Yu, Y., 2008. ENSO at 6ka and 21ka from ocean–atmosphere coupled simulations. *Clim. Dynamics* 30, 745–762. doi:10.1007/s00382-007-0320-3.